Developmental Cell, Vol. 5, 217–230, August, 2003, Copyright ©2003 by Cell Press

Control of Skeletal Patterning by EphrinB1-EphB Interactions

Amelia Compagni,[1] Malcolm Logan,[2] Rüdiger Klein,[3] and Ralf H. Adams[1,*]

[1]Cancer Research UK London Research Institute
Vascular Development Laboratory
London WC2A 3PX
United Kingdom

[2]National Institute for Medical Research
Division of Developmental Biology
London NW7 1AA
United Kingdom

[3]Max-Planck Institute of Neurobiology
Department of Molecular Neurobiology
D-82152 Martinsried
Germany

Summary

We report that targeted inactivation of the Eph receptor ligand ephrinB1 in mouse caused perinatal lethality, edema, defective body wall closure, and skeletal abnormalities. In the thorax, sternocostal connections were arranged asymmetrically and sternebrae were fused, defects that were phenocopied in EphB2/EphB3 receptor mutants. In the wrist, loss of ephrinB1 led to abnormal cartilage segmentation and the formation of additional skeletal elements. We conclude that ephrinB1 and B class Eph receptors provide positional cues required for the normal morphogenesis of skeletal elements. Another malformation, preaxial polydactyly, was exclusively seen in heterozygous females in which expression of the X-linked *ephrinB1* gene was mosaic, so that ectopic EphB-ephrinB1 interactions led to restricted cell movements and the bifurcation of digital rays. Our findings suggest that differential cell adhesion and sorting might be relevant for an unusual class of X-linked human genetic disorders, in which heterozygous females show more severe phenotypes than hemizygous males.

Introduction

The assembly and segmentation of mesenchymal condensations and their differentiation into cartilage and bone are critical processes in the development of the vertebrate skeleton. In the embryonic thorax, paired ribs extend from the vertebral column and connect to two condensed mesodermal bars, termed sternal bands, which will subsequently migrate toward the ventral midline and fuse to form the sternum. Concomitantly, the sternum becomes cartilaginous and eventually ossifies into segmented sternebrae, but not at sternocostal joints where ribs are connected (Chen, 1952). During limb development, blocks of condensed mesenchyme are modeled into precisely shaped cartilaginous elements through steps of segmentation and bifurcation before endochondrial ossification commences (Shubin and Alberch, 1986). The relevance of these processes is most evident in the distal limb, the autopod, which comprises numerous small carpal/tarsal bones and the phalanges of the digits.

Although the significance of mesenchymal condensations has been long recognized, relatively little is known about the molecular mechanisms controlling the patterning processes described above. Previous work has shown that cell adhesion and extracellular matrix molecules, such as N-CAM, N-cadherin, and proteoglycans, contribute to the initial formation of condensations and the subsequent separation of perichondreal and periosteal cells from the surrounding mesenchyme (Hall and Miyake, 2000). TGF-β superfamily growth factors, such as bone morphogenetic proteins (BMPs) and growth and differentation factors (GDFs), control multiple aspects of skeletogenesis, including the subdivision of skeletal elements by joints (Storm and Kingsley, 1996).

Eph receptor tyrosine kinases (RTKs) and ephrin ligands are versatile regulators of embryonic morphogenesis. Sequence homology and ligand binding preferences separate the 14 Eph receptors known in higher vertebrates into two subclasses, EphA and EphB receptors. EphB RTKs (EphB1–EphB6) signal in combination with B class ephrins (ephrinB1–ephrinB3), transmembrane proteins with a short yet highly conserved cytoplasmic domain. Remarkably, ephrins not only function as conventional ligands, but also are themselves capable of receptor-like signal transduction (Kullander and Klein, 2002). Known biological functions of Eph/ephrin molecules include the patterning of hindbrain and somites, cell sorting in the intestine, the guidance of neural crest cells to their target regions, the wiring of neuronal connections in the nervous system, and the formation of blood vessels. In many of these processes, Eph-ephrin signaling appears to generate repulsive or nonpermissive cues. For example, neuronal growth cones utilize Eph RTKs and ephrins to disengage from unsuitable targets. In a similar fashion, Eph receptors and ephrins expressed in a complementary pattern in the rhombomeres of the hindbrain restrict cell movement and intermingling at the segment boundaries (Wilkinson, 2001; Kullander and Klein, 2002; Batlle et al., 2002).

Here we describe that B class ephrins and their cognate Eph receptors play a role in the patterning of the developing skeleton. To study the in vivo function of ephrinB1, we have generated conditional mutant mice using the Cre-loxP approach. As the *ephrinB1* gene is X-linked in mice and humans, Cre-mediated deletion of the conditional *ephrinB1Lox* allele produced hemizygous males (ephrinB1^{KO}) and heterozygous females (ephrinB1$^{KO/+}$), most of which died during late gestation or shortly after birth. All ephrinB1-deficient mutants displayed a range of malformations affecting rib pairing at sternocostal joints, sternum segmentation, and patterning of carpal bones in the autopod. One other defect, preaxial polydactyly, was confined to mosaic heterozygous females in which cells utilized either the wild-type

*Correspondence: ralf.adams@cancer.org.uk

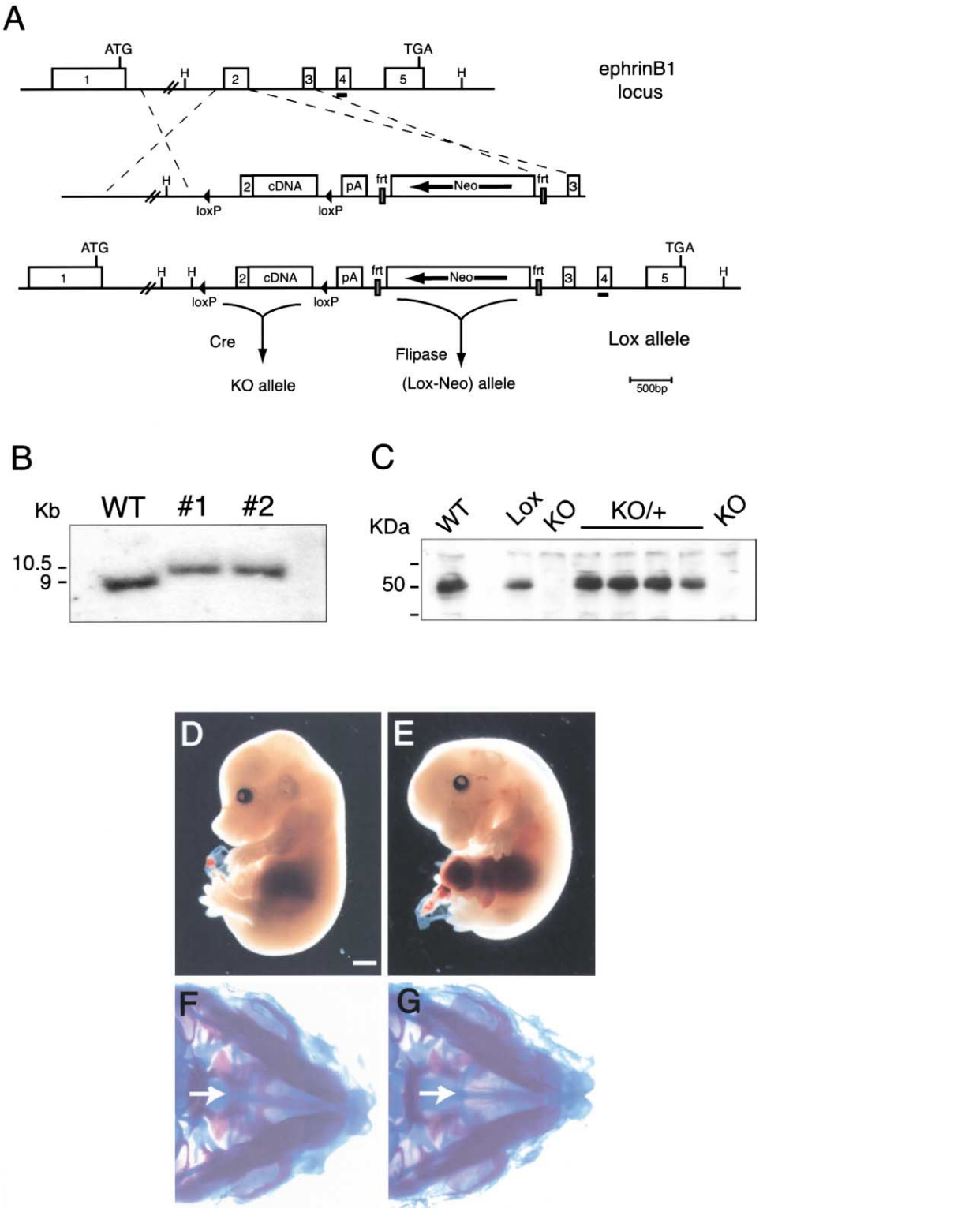

Figure 1. Generation of EphrinB1 Mutants

(A) Scheme of the mouse *ephrinB1* gene, targeting vector, and targeted locus. Exon 2 was flanked by loxP sites (black triangles) and fused to a human ephrinB1 cDNA with polyadenylation signal (pA). The neomycin resistance cassette (Neo) in conditional (Lox) mice was removed by Flp-mediated recombination on frt sites (gray boxes) resulting in an (Lox-Neo) allele. LoxP sites allowed Cre-mediated inactivation of the *ephrinB1* gene (KO). HindIII sites and the Southern probe (line below exon 4) are shown.

(B) Homologous recombination in ES cells was verified by Southern hybridization on genomic DNA cut with HindIII. The probe from exon 4 detected a 9 kb band in the wild-type allele (WT) and a single 10.5 kb band in two targeted (hemizygous) clones (1 and 2).

or the disrupted *ephrinB1* allele because of X inactivation. Our analysis of mutant mice revealed that EphB-ephrinB interactions are necessary for patterning and, if provided in the right context, sufficient to impose splitting/branching on mesenchymal condensations.

Results

Conditional Inactivation of the *ephrinB1* Gene

The *ephrinB1* gene is located on the X chromosome in mice and humans. As expression of *ephrinB1* in embryonic stem (ES) cells and embryos has been previously reported (Bouillet et al., 1995), we decided to target the gene by a conditional (Cre-loxP) strategy (Figure 1A and Experimental Procedures). PCR and Southern blot analysis confirmed homologous recombination in ES cell clones. Two independent mouse lines with a loxP-flanked *ephrinB1* gene were generated (Figure 1B). Heterozygous (ephrinB1$^{Lox/+}$), homozygous (ephrinB1$^{Lox/Lox}$), and hemizygous (ephrinB1^{Lox}) offspring proved to be viable and fertile. However, a small fraction of homozygous or hemizygous mice ($\sim$10%) died within 24 hr after birth, apparently because of cleft palate defects. To generate ephrinB1-deficient mice, conditional (Lox/+ or Lox/Lox) mutants were bred to PGK-Cre transgenic animals (Lallemand et al., 1998). Successful deletion of the loxP-flanked area in the *ephrinB1* gene and absence of the gene product were confirmed for all lines by PCR and Western blotting (Figure 1C and data not shown). Whereas no ephrinB1 protein was detectable in male hemizygous null mutants (ephrinB1^{KO}), ephrinB1 expression in heterozygous KO/+ females was comparable to wild-type controls and above levels observed in conditional homozygous/hemizygous mice.

Crossbreeding of ephrinB1 conditional and PGK-Cre mice produced very few viable ephrinB1-deficient animals, and only about 15% of the expected number of knockout males were present at weaning age. Surprisingly, ephrinB1$^{KO/+}$ females were even more compromised, and only 1%–2% survived. EphrinB1$^{KO/+}$ heterozygotes presented a mosaic situation in which areas lacked ephrinB1 expression because of X inactivation, a mechanism by which each cell of the female postimplantation embryo stochastically silences one X chromosome to control gene dosage (Avner and Heard, 2001; Hadjantonakis et al., 2001). X inactivation is stable and passed on clonally to all progeny during later cell divisions, hence producing a mosaic pattern.

We next isolated embryos at different stages of development to identify the cause for the lethality of ephrinB1-deficient animals. Mutant embryos were readily recovered from all stages between midgestation and birth, although we found a few dead heterozygotes/hemizygotes after embryonic day 12.5 (E12.5). Freshly isolated ephrinB1 mutants at E14.5 displayed multiple defects, including edema in the back region, incomplete body wall closure (omphalocele), cleft palate, and shortening of the skull (Figures 1D–1G and data not shown). Several of these malformations were severe enough to account for the predominant postnatal lethality of mutants. Consistent with the very low survival rate observed for ephrinB1$^{KO/+}$ females, defects in the ventral body wall were most prominent and fully penetrant in heterozygotes. Since a small number of ephrinB1-deficient mice reached adulthood and proved fertile, we were able to generate a few litters containing homozygous females (ephrinB1$^{KO/KO}$). The appearance of these embryos was very similar to hemizygous male knockouts, indicating that phenotypic differences were not gender dependent (data not shown).

Asymmetric Rib Pairing and Sternebral Fusions in EphrinB1 and EphB Mutants

The observation that ephrinB1 mutants presented cleft palate prompted us to look for additional alterations in their skeletons. At E18.5, alizarin red/alcian blue preparations revealed asymmetric pairing of the ribs in ephrinB1^{KO} males and, to a lesser extent, in ephrinB1$^{KO/+}$ females (Figures 2A–2C and Table 1). Sternocostal junctions were abnormally positioned, and the ossification centers that give rise to the distinct sternal segments appeared expanded and fused (Figures 2B and 2C). Abnormal ossification patterns were also observed in correspondence to normally paired ribs, suggesting involvement of ephrinB1 in different steps of sternal development (Figures 2B and 2C and data not shown). Histological analysis of the sternum in ephrinB1 mutant embryos confirmed that the insertion of ribs was asymmetric and showed that the fusion of the two sternal bands at the body midline was incomplete at E15 (Figures 2D–2F). Whole-mount in situ hybridization at E12.5 for *collagen2a*, a differentiation marker for condensing mesenchyme, revealed that ephrinB1^{KO} sternal bands remained diffuse and poorly delineated, and the gap between the lower ribs and the sternum appeared greater than in wild-type embryos (Figures 2G–2H). These observations suggested that the attachment of ribs to sternal bands and, later, sternum formation were delayed in the absence of ephrinB1.

The receptors EphB2 and EphB3 are important interaction partners of ephrinB1, and a fraction of EphB2 KO/EphB3 KO double mutants developed cleft palate and umbilical herniation (Orioli et al., 1996), defects reminiscent of ephrinB1-deficient mice. These similarities prompted us to analyze the thoracic skeleton of EphB2 and EphB3 mutants. While single knockout embryos did not present appreciable alterations, mild patterning defects in the thoracic skeleton were already observed in double heterozygotes (Figures 2I and 2J), indicating some degree of functional redundancy. Complete loss of both receptors reproduced the skeletal defects seen

(C) Western blot analysis for ephrinB1 protein in E12.5 embryos after PGK-Cre-mediated inactivation of the gene. Glycosylated proteins were enriched by wheat germ agglutinin (WGA) pull-down. No ephrinB1 protein was detected in KO males. Levels of ephrinB1 in KO/+ females were comparable to those in WT embryos.

(D and E) Freshly dissected ephrinB1mutants at E14.5 displayed dorsal edema, omphalocele, and cleft palate. The latter is clearly visible in alizarin red/alcian blue skeletal preparations ([F and G], arrows). The scale bar represents 1 mm in (D) and (E) and 0.5 mm in (F) and (G).

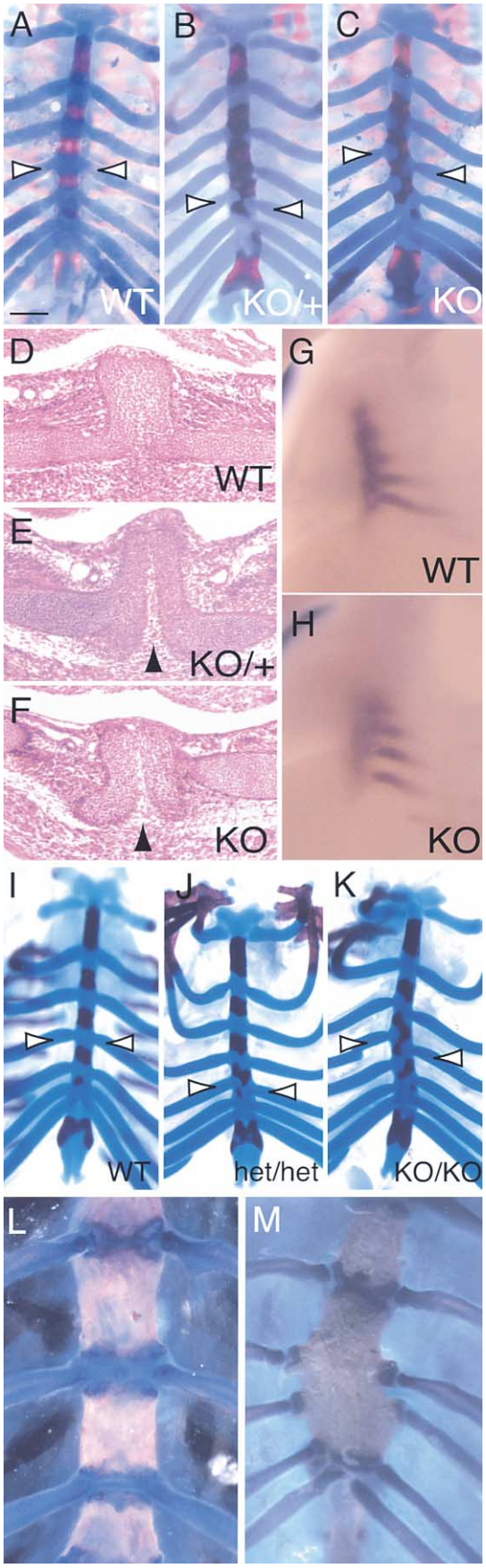

in ephrinB1^{KO} mice, i.e., asymmetric arrangement of sternocostal junctions and fusion of ossified sternebrae (Figure 2K). Consistent with what was observed during embryonic development, the few ephrinB1^{KO} males surviving to adulthood all presented a severely malformed sternum of reduced length and with fused sternebrae ($n = 6$; Figures 2L and 2M).

Analysis of the expression of ephrinB1 and its receptors, EphB2 and EphB3, supported a functional role of these molecules in the development of the rib cage. Whole-mount in situ hybridization showed expression of *ephrinB1* in correspondence with the sternal bands and around the tip of the ribs (Figure 3A). Immunofluorescent detection on sections of E12.5 embryos confirmed the presence of ephrinB1 protein around the areas of rib-sternum contact, sites at which the ribs elongate and are pulled toward the midline, and in muscles in close proximity to the rib cage (Figures 3B–3D). The sternal bands and the rib perichondrium were positive for EphB2 expression both by immunofluorescent detection and β-galactosidase staining in mice carrying an *EphB2LacZ* knockin allele (Henkemeyer et al., 1996) (Figures 3E–3G). Moreover, EphB2 was prominently expressed in tissues surrounding the inner perimeter of the rib cage, including the mesothelial lining of the thorax (Figure 3E). After sternum fusion, EphB2 expression was restricted to the sternal midline and intercostal muscles (Figure 3H). EphB3 protein appeared to be expressed in chondrogenic cells of the developing ribs and skull (data not shown).

In conclusion, our expression analysis suggests that ephrinB1-EphB interactions might occur predominantly at the distal end of growing ribs, within the sternal band mesenchyme, and at the sternocostal junctions (Figure 3D), consistent with the skeletal defects described above.

Limb Defects in EphrinB1 Mutants

Examination of freshly dissected ephrinB1 embryos revealed another skeletal defect, namely polydactyly, that almost exclusively affected digits I or II (Figures 4A and 4B). The phenotype occurred equally in forelimbs and

Figure 2. Sternum Development Is Disturbed in EphrinB1 Mutants

(A–C) Alizarin red/alcian blue preparations of E18.5 rib cages in wild-type (A), KO/+ (B), and KO (C) embryos. Corresponding ribs insert asymmetrically into the sternum in KO and KO/+ animals (arrowheads), and the ossification pattern of the sternum is altered.

(D–F) Hematoxilin/eosin staining of transversal sections of wild-type (D), KO/+ (E), and KO (F) embryos at E14.5. In ephrinB1 mutants the fusion of the sternum is incomplete (arrowheads).

(G and H) In situ hybridization of *collagen2a* in wild-type (G) and KO (H) embryos. Note diffuse staining corresponding to the sternum in ephrinB1 mutants.

(I–K) Alizarin red/alcian blue skeletal preparations of rib cages from wild-type (I), double heterozygous EphB2/EphB3 (J), and EphB2/EphB3 double knockout E18.5 embryos (K). Arrowheads indicate the asymmetric pairing of the ribs.

(L and M) Skeletal preparations of adult rib cages of wild-type (L) and KO (M) animals. The early defects result in fusion of the lower sternebrae and shortening of the sternum.

The scale bar represents 700 μm in (A), (B), (I)–(K), (L), and (M) and 190 μm in (G) and (H); (D–F) 40×; (G and H) ventral corresponds to left and dorsal corresponds to right.

Table 1. Summary of Defects in Embryonic Sternum and Adult Limbs

Sternum Phenotypes (E17.5–18 Embryos)

Phenotypes	EphrinB1 KO (n = 11)	EphrinB1 KO/+ (n = 8)	EphrinB1 Lox/+ (n = 7)	EphrinB1 WT/Lox (n = 8)
Rib mispairing	5	3	2	0
Sternebrae fusion	6	3	1	0
Incomplete sternum fusion	0	2	0	0

Summary of Carpal Defects (Adult Mice)

Phenotypes	EphrinB1 KO (n = 5)	EphrinB1 KO/+ (n = 1)	EphrinB1 WT/Lox (n = 3)
Fusion (3 + 2)	4	1	0
Extra ossifications	4	1	0

The number of affected mutants for each phenotype is given together with the total number of animals analyzed (in parentheses).

hindlimbs and was often accompanied by syndactyly. Only in very rare cases did other digits show similar defects, normally at the level of the last phalange (Figure 4C). Alizarin red/alcian blue preparations at E18.5 revealed that the extra skeletal elements were generated by bifurcation of digits at variable positions along the proximal-distal axis. The phalanges proximal to branch points were in some cases broader than normal, suggesting delayed separation of the bifurcated region (Figure 4C). Surprisingly, polydactyly affected exclusively heterozygous ephrinB1$^{KO/+}$ females (75% penetrance). Alcian blue staining allowed us to examine cartilage formation at earlier stages (Figures 4D–4F). Starting from E12, we frequently observed that autopods of ephrinB1 heterozygotes contained extra cartilaginous elements, which were either generated by branching of digits (Figure 4E) or appeared as isolated clusters in the interdigital space underneath the apical ectodermal ridge (AER; data not shown). In contrast, ephrinB1^{KO} limbs did not present prominent abnormalities in the developing digits (Figures 4D and 4F).

Previous work has demonstrated that the Prx1 limb enhancer is particularly suitable to direct expression to limb mesenchyme (Martin and Olson, 2000). We made use of a Prx1-Cre transgenic line (Logan et al., 2002) to generate limb-specific ephrinB1 knockouts (ephrinB1$^{\Delta limb}$). Hemizygous/heterozygous ephrinB1$^{\Delta limb}$ mutants no longer showed omphalocele or other defects. However, limb-specific inactivation of the ephrinB1 gene led to preaxial polydactyly in heterozygous females, reproducing our previous findings (Figures 4G–4I).

Several studies have implicated Sonic hedgehog (Shh) and its pathway in the development of polydactyly (Capdevila and Izpisua Belmonte, 2001). By whole-mount in situ hybridization, we could not detect any changes in the pattern of expression of *Shh*, its receptor *Patched1* (*Ptc1*), or two modulators of this signaling pathway, *Gli1* and *Gli3*, in heterozygous females. Moreover, expression of *FGF4* and *FGF8*, labeling the AER, was not expanded to the anterior part of the limb (see Supplemental Data at http://www.developmentalcell.com/cgi/content/full/5/2/217/DC1; data not shown). Thus, we concluded that the mechanism generating preaxial polydactyly in ephrinB1$^{KO/+}$ females was Shh independent.

Having observed patterning defects in the mutant rib cage and polydactyly, we next examined the joints in digits and in the carpal bones of wrists, areas in which small bones are formed from mesenchymal condensations through segmentation. Surviving adult ephrinB1^{KO} animals showed several defects in the wrist skeleton, most prominently the fusion of distal carpal bones and the formation of ectopic ossifications. Such additional skeletal elements occurred typically in posterior limbs and were either attached or in close proximity to triquetral and hamate bones (Figures 4O and 4P and Table 1). Skeletal preparations at E18.5 confirmed that separation of the cartilages corresponding to the distal carpal bones was delayed or sometimes impaired in both ephrinB1^{KO} and ephrinB1$^{KO/+}$ embryos (data not shown). Consistent with a role in the organization and segmentation of carpal primordia, ephrinB1 protein was observed within prechondrogenic condensations (Figures 4J and 4M and Flenniken et al., 1996), whereas the receptors EphB2 and EphB3 were presented on adjacent nonchondrogenic mesenchymal cells (Figures 4K–4M). EphrinB1 was significantly downregulated during later stages of development, but EphB receptor expression persisted in tissues surrounding and separating cartilaginous condensations as well as in the perichondrium (Figure 4N and data not shown). In digits, ephrinB1 was absent from condensations and interphalangeal joints, and, as one would expect, joint morphology and expression of the marker *Gdf5* appeared unaltered in mutant embryos (data not shown).

The above findings indicated that ephrinB1 is required for the correct segmentation of skeletal elements. Expecting to learn more about the functional role of Eph/ephrin molecules in patterning processes, we decided to investigate the mechanism through which mosaic expression of the X-linked *ephrinB1* gene could induce polydactyly in heterozygous mutants.

Mosaic Expression of EphrinB1 Generates Ectopic Signaling Interfaces

Whole-mount in situ hybridization of embryos carrying a loxP-flanked *ephrinB1* gene confirmed the known pattern of *ephrinB1* expression in the distal limb mesenchyme underneath the AER (Figure 5A and Flenniken et al., 1996). Patches of *ephrinB1*-deficient cells were visible in ephrinB1$^{KO/+}$ limbs but appeared underrepresented in comparison to what was expected for random X inactivation, and large domains of mesenchyme expressed the ligand (Figures 5B and 5C). At the same time, staining was more intense than normal in the positive cells, indicating that *ephrinB1* transcript levels were elevated. This was also true for many other *ephrinB1*-expressing tissues in the embryo (Figures 5B and 5C

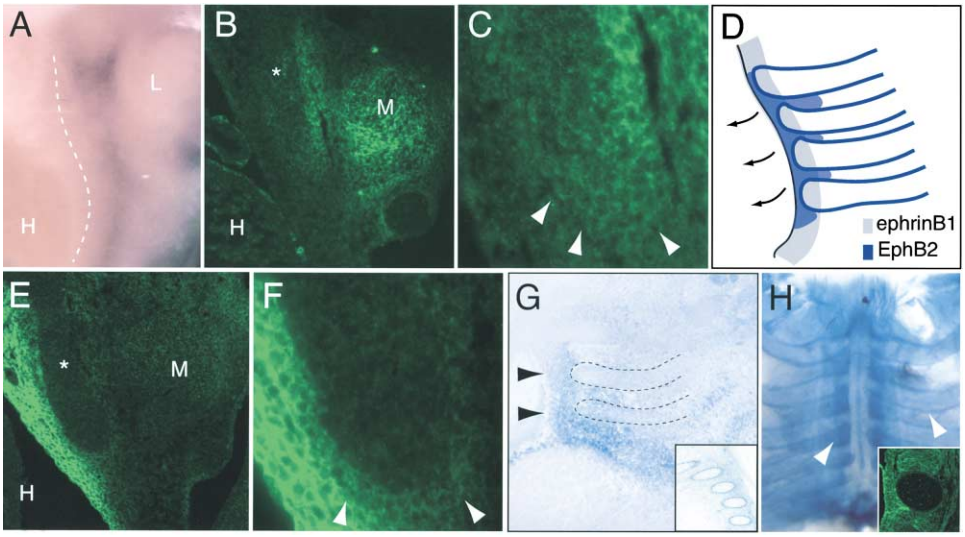

Figure 3. Distribution of EphrinB1 and EphB2 in the Forming Rib Cage

(A) Whole-mount in situ hybridization of *ephrinB1* at E12.5. The sternal band is indicated by the dotted line.

(B and C) Immunofluorescent detection of ephrinB1 protein in transverse sections of E12.5 embryos. EphrinB1 is distributed at the tip of the rib (arrowheads).

(D) Scheme summarizing ephrinB1 and EphB2 expression and interaction areas. Arrows indicate the movement of the sternal bands toward the midline.

(E and F) Immunofluorescent detection of EphB2 protein in transverse sections of E12.5 embryos. EphB2 labels the rib perichondrium (arrowheads) and the mesothelial lining of the thorax.

(G and H) Distribution of EphB2 by EphB2LacZ staining.

(G) Tangential 10 μm section of E12.5 embryo after LacZ staining, showing EphB2 in the sternal band (arrowheads) and the rib perichondrium (inset). Dotted lines highlight the ribs.

(H) Whole-mount LacZ staining of E14.5 rib cage. EphB2 is localized to the intercostal muscles (arrowhead and inset), along the rib perichondrium (arrowhead), and at the site of sternum fusion (midline).

(B and E) The rib is indicated by an asterisk.

H, heart; M, muscle; L, limb; (B and E) 20×; (C and F) 63×; (G) 5×.

and data not shown) and consistent with the comparable ephrinB1 protein levels seen in wild-type and KO/+ mice (Figure 1C).

EphrinB1 can interact and signal in combination with the receptor EphB2, and both molecules show overlapping expression in the mesenchyme underneath the AER (Figures 5A and 5D and data not shown). In ephrinB1^{KO} males, EphB2LacZ staining revealed the normal pattern of expression, but with increased intensity compared to wild-type limbs, indicating some degree of receptor upregulation (Figures 5D and 5E). Expression of the β-galactosidase reporter in ephrinB1 KO/+ females was strikingly mosaic (Figures 5F and 5G), and the few domains with high levels of EphB2LacZ staining corresponded to clusters of *ephrinB1*-deficient cells. In situ hybridization showed that *EphB3* transcripts were also distributed in a mosaic pattern in heterozygous ephrinB1 mutants (Figures 5H and 5I), denoting that changes in receptor expression were at least partially controlled at the transcript level.

X inactivation in living mice or isolated tissues can be efficiently visualized with the help of an X-linked GFP transgene (X-GFP; Hadjantonakis et al., 2001). We generated ephrinB1 KO/+ heterozygous animals in which the wild-type X chromosome carried the GFP transgene, hence permitting identification of cells with (GFP positive) or without (GFP negative) a functional *ephrinB1* gene. Confirming the upregulated expression of EphB receptors in ephrinB1-deficient cells, a soluble fusion protein consisting of the ephrinB1 extracellular domain and the human secreted alkaline phosphatase (ephrinB1-AP) showed strong binding to the GFP-negative distal mesenchyme, but not to the adjacent fluorescent areas (Figures 6A–6C). Likewise, EphB2LacZ staining was restricted to clusters of ephrinB1 KO cells (data not shown). Hence, expression of ephrinB1 and its receptors was complementary, and receptor-ligand interactions were confined to the boundaries of mosaic areas.

In X-GFP ephrinB1$^{KO/+}$ females, fluorescent and GFP-negative mesenchymal cells were organized in alternating stripes extending from the distal edge of limb buds along the proximal-distal axis (Figures 6A and 6D), reminiscent of cellular fate maps established by dye tracing studies in chick (Vargesson et al., 1997). We observed that bifurcations occurred when interfaces between ephrinB1- and EphB-expressing mesenchyme were placed at the tip of forming digits. This involved either juxtaposition of two complementary mosaic areas or intercalation of ephrinB1-deficient cells into GFP-positive mesenchyme (Figures 6E and 6F). Common to both scenarios is that ectopic interfaces of receptor-ligand signaling were positioned perpendicular to the AER, thereby intersecting the growing end of a digital ray. We also examined EphB2 receptor activation in mutant embryos. Only weak receptor tyrosine phosphorylation

could be seen in ephrinB1 knockout males, indicating that the ligand is a prominent activator of EphB2. As one would expect for mosaic mutants, receptor activation levels in ephrinB1$^{KO/+}$ heterozygotes were variable and intermediate compared to ephrinB1 knockouts and wild-type controls (Figure 6G). These findings show that, in KO/+ mice, EphB-ephrinB1 signaling was neither generally lost nor enhanced, but, rather, restricted to few interaction areas.

EphB-EphrinB Signaling Restricts Cell Movements

To address the mechanism generating polydactyly in female mutants, we investigated whether EphB-ephrinB1 signaling in the mesenchyme could lead to increased cell proliferation or reduced apoptosis, two mechanisms which might create a local surplus of chondrogenic cells and lead to the formation of extra digits. However, our analysis revealed that levels of cell division in the distal mesenchyme were similar in ephrinB1-expressing and -deficient areas of KO/+ limbs and comparable to wild-type embryos (Supplemental Data). Likewise, apoptosis appeared to be generally unaffected in mutant hand plates, but significantly fewer apoptotic nuclei were detected at bifurcations compared to normal interdigital zones (IDZs), in agreement with the observation that bifurcated digits were mostly syndactylous (Supplemental Data).

Formation of ectopic digits might reflect a shift in the responsiveness of cells to cartilage-promoting signals. In order to test whether the loss of the *ephrinB1* gene might affect this process, we studied the chondrogenic capability of mutant limb mesenchyme in high-density cell culture. Alcian blue staining of differentiating nodules showed that comparable numbers of chondrogenic clusters were produced in mutant and control cultures (Figures 7A–7C), and we concluded that ephrinB1 is not essential for the induction or suppression of the chondrogenic cell fate.

The transcription factor Sox9 is a marker for condensing mesenchyme and the cartilage lineage and is normally not expressed in interdigital spaces. In bifurcated digits, *sox9*-positive cells were unexpectedly found in the newly formed IDZ (Figures 7D–7F). This indicated that ephrinB1-EphB interactions at the digit tip induced splitting of the chondrogenic mesenchyme by a mechanism dominant over the normal differentiation pathway.

Eph receptors and ephrins can mediate boundary formation and restrict cell migration by providing repulsive signals (Wilkinson, 2001). In limbs of wild-type females carrying an X-GFP allele, the distal mesenchyme showed a large degree of cell mixing, as revealed by the intermingling of GFP-positive and -negative cells (Figures 7G and 7J). In contrast, the two cell populations were clearly separated and arranged in distinct domains in ephrinB1 KO/+ mutants (Figures 7I and 7L). Due to the reduced ephrinB1 expression and EphB2 tyrosine phosphorylation (Figures 1C and 6G), conditional (Lox) mice constituted a hypomorphic situation, and, consistently, a small proportion (10%) of ephrinB1$^{Lox/+}$ heterozygotes developed preaxial polydactyly. Analysis of the X-GFP pattern in Lox/+ animals showed intermediate levels of cell intermingling in comparison to WT and KO/+ limbs (Figures 7H and 7K). Moreover, while boundaries between areas utilizing the wild-type and the targeted X chromosomes were sharp in ephrinB1$^{KO/+}$ embryos, they appeared more irregular in Lox/+ littermates (Figures 7K and 7L). Thus, mosaic expression of the X-GFP transgene revealed a significant extent of cell movement and intermingling in the wild-type limb mesenchyme, which became significantly restricted across interfaces of ligand-receptor interaction in ephrinB1 KO/+ mice and, to a lesser extent, in hypomorphic Lox/+ females. In conclusion, our results suggest that ectopic EphB-ephrinB1 interactions at mosaic interfaces are sufficient to induce ectopic branching or splitting of chondrogenic condensations by generating a repulsive signal that restricts cell movements. Similar signals appear to play important roles in the normal segmentation and patterning of chondrogenic condensations, since the loss of ephrinB1 or EphB receptors in mutant mice resulted in segmentation defects of the axial and appendicular skeleton.

Discussion

Development of the vertebrate skeleton involves the migration of mesenchymal cells to the sites of skeletogenesis and their aggregation into condensed blocks, which are further shaped by polarized growth and segmentation before they differentiate into the chondroblastic lineage (Shubin and Alberch, 1986; Hall and Miyake, 2000). Here we have demonstrated that ephrinB1 and EphB receptor tyrosine kinases play important roles in the patterning of skeletal elements by controlling cell-cell interactions at sites where mesenchymal condensations grow, divide, or fuse.

EphB-EphrinB Interactions Contribute to Skeletal Development

Our analysis of ephrinB1 mutant mice uncovered a range of malformations affecting the axial and appendicular skeleton, such as asymmetric attachment of ribs, lack of joints in sternum and limbs, and preaxial polydactyly. Common to all was an underlying abnormal segmentation of mesenchymal condensations, being either missing or, vice versa, ectopic.

In the thorax, expression patterns and malformations in mutant mice suggest that EphB-ephrinB1 interactions might assist the condensation of sternal bands and fusion of the sternum at the ventral midline. EphrinB1 and EphB2 proteins were also found at the distal end of ribs, and here their interaction might contribute to the formation of the sternocostal junctions, e.g., by positioning the sites of rib attachment. Prominent expression of these molecules was also found in tissues enclosing the elongating rib processes and, in the case of EphB2, in intercostal muscles. Future work will have to address whether Eph-ephrin signaling between ribs and muscle or other surrounding tissues contributes to the mutant phenotypes.

EphrinB1 and EphB2/EphB3 mutants displayed fusion of sternebrae. Factors such as GDF5 and BMP5 were reported to coordinate the formation of sternebrae and sternocostal junctions (Storm and Kingsley, 1996). Although asymmetrical rib attachment might be a major

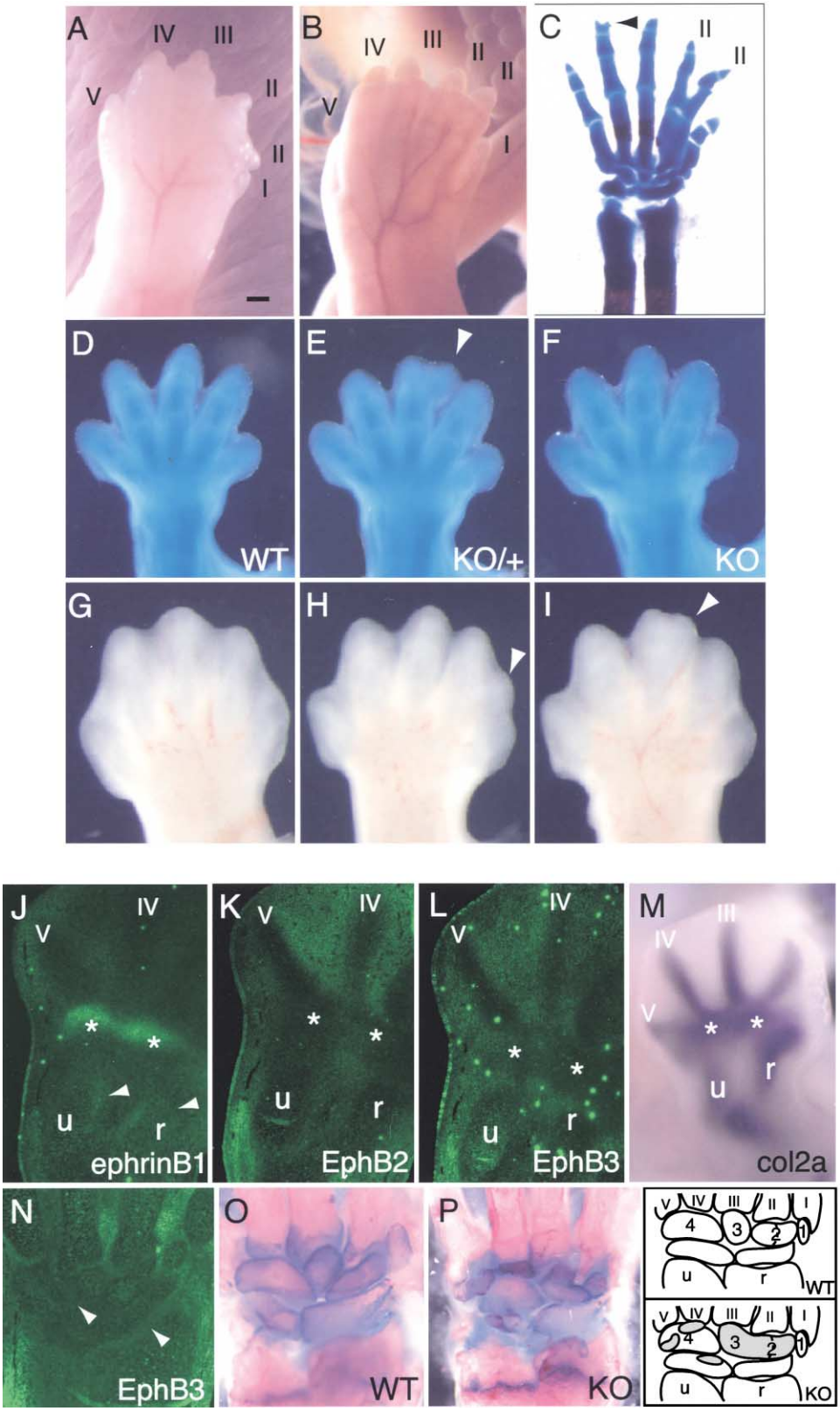

Figure 4. EphrinB1 Mutants Display Limb Defects

Freshly dissected ephrinB1 KO/+ forelimb (A) and hindlimb (B) at E16.5 showing duplication of digit II. Digits are labeled I–V in anterior-posterior order.

cause for abnormal sternum ossification in ephrinB1 mutants, similar defects also occurred at normally paired ribs (Figure 2M and data not shown), suggesting that, in this process, Eph/ephrin molecules might act in parallel or in combination with GDF/BMP proteins. A similar connection might be valid for the morphogenesis of the wrist, where a role for GDF5 and related proteins has been reported (Storm and Kingsley, 1996).

In developing limbs, ephrinB1 protein was transiently concentrated in condensed mesenchyme corresponding to future carpal bones, while EphB receptors were mainly expressed in a complementary fashion in surrounding tissues and in the perichondrium. These expression patterns suggest that interactions between opposing cells expressing either ephrinB1 or EphB RTKs generate local signals required for the correct patterning of condensations. Mutant phenotypes such as the fusion of bones and the presence of small ectopic ossifications, which might be the product of aberrant separations from larger condensations or incorrect sorting of prechondrogenic cells, support a role of ephrinB1-EphB interactions in the process of segmentation. In contrast, our analysis indicated that the initial aggregation of cells into condensed blocks of mesenchyme and the growth of condensations were not significantly dependent on ephrinB1.

Induction of Polydactyly at Ectopic EphB-EphrinB Signaling Interfaces

One additional skeletal abnormality, the branching of digital rays and the resultant preaxial polydactyly, was confined to heterozygous ephrinB1$^{KO/+}$ females. Whereas expression patterns for ephrinB1 and B class receptors were partially overlapping in the distal limb mesenchyme and at digit tips in normal embryos, the mosaic loss of ephrinB1 in KO/+ limbs led to strictly complementary expression of EphB receptors. Moreover, both ligand and receptors appeared upregulated in their respective mosaic domains. An appealing explanation for these alterations in heterozygotes might be that compensatory mechanisms tried to restore normal levels of signaling in the absence of ephrinB1. Conversely, EphB receptor expression might be lowered in the presence of high ephrinB1 levels as a response to transiently enhanced Eph-ephrin signaling.

Because of the mosaic and complementary expression of ephrinB1 and its receptors in heterozygous mutants, new ectopic receptor-ligand interfaces were established. Signals from these interfaces, when positioned centrally at digit tips, were sufficient to split mesenchymal condensations and induce bifurcations. Similar interactions between juxtaposed cell populations appear to control normal patterning processes, since complementary expression of Eph and ephrin molecules occurs in the carpal mesenchyme, and segmentation in wrists was defective in the absence of ephrinB1. The lack of evident digit abnormalities in ephrinB1 KO males indicated that differences were either very subtle or counteracted by compensatory mechanisms, promoted, for example, by other ephrins.

Patterning of Condensations through Repulsive Signals

How can ephrinB1-EphB interactions regulate segmentation and patterning processes? One possibility might be that enhanced proliferation of chondrogenic cells leads to a size expansion of cartilaginous condensations and eventually triggers the bifurcation of digits. Arguing against such a passive growth-controlled mechanism, ephrinB1 mutant limbs did not contain enlarged skeletal elements, and numbers of proliferating cells were comparable between mosaic areas. A previous study has also shown that the A class receptor EphA7 facilitates chondrogenic condensation (Stadler et al., 2001), but ephrinB1 KO, KO/+, and control mesenchyme showed very similar chondrogenic capacities. Furthermore, we found that the polydactyly in ephrinB1 KO/+ limbs was independent from changes in the Shh pathway.

We also observed that IDZs forming between bifurcated digits in ephrinB1 KO/+ mutants were largely devoid of programmed cell death. BMPs and their receptors regulate apoptosis of interdigital cells (Capdevila and Izpisua Belmonte, 2001), and, indeed, transcripts for *bmp2*, *bmpr-1a*, and *msx-1* were initially absent in ectopic IDZs, which instead showed residual expression of the chondrogenic marker *sox9*. This indicated that morphological alterations induced by ectopic EphB-ephrinB1 signaling preceded and were, to a certain extent, independent from changes in the genetic programs controlling the development of digits and IDZs.

Previous work has shown that the Eph/ephrin system plays important roles in the guidance of neuronal growth cones and migrating cells by providing repulsive cues (Wilkinson, 2001; Kullander and Klein, 2002). Moreover, complementary patterns of Eph and ephrin expression in adjacent hindbrain rhombomeres are critically involved in restricting cell movement and intermingling,

(C) Limb skeletal preparation by alizarin red/alcian blue staining of a KO/+ mutant at E18.5. Note duplication of digit II and the minor alteration at the digit tip in position IV (arrowhead).

(D–F) Example of digit bifurcation (arrowhead) in an alcian blue-stained KO/+ limb at E13.5.

(G–I) Freshly dissected E12.5 wild-type (G) and mutant (H and I) limbs after Prx1-Cre-mediated deletion of ephrinB1 (ephrinB1$^{\Delta limb}$).

(J–L) Immunofluorescent detection of ephrinB1 (J), EphB2 (K), and EphB3 (L) in the developing carpal region of E12.5 limbs (5 μm sections). Asterisks correspond to the prechondrogenic masses of the carpal elements as confirmed by *collagen2a* whole-mount in situ hybridization (M). Note the presence of ephrinB1 staining (arrows) on the distal ends of ulna (u) and radius (r). Digits III–V are labeled.

(N) Detection of EphB3 receptor in E13.5 limb sections. EphB3 persists around the carpal cartilages (arrows) and at sites of joint formation at later stages (data not shown).

(O and P) Skeletal preparations by alizarin red/alcian blue staining of WT (O) and KO (P) adult limbs. As schematized (right bottom panel), mutant capitate (3) and trapezoid/central (2) bones were fused, and extra ossifications were connected or formed in correspondence to hamate (4) and triquetral.

The scale bar represents 250 μm in (A)–(C), 230 μm in (D)–(F), 180 μm in (G)–(I) and (M), and 450 μm in (O) and (P); (J–N) 10×; anterior corresponds to right and posterior corresponds to left.

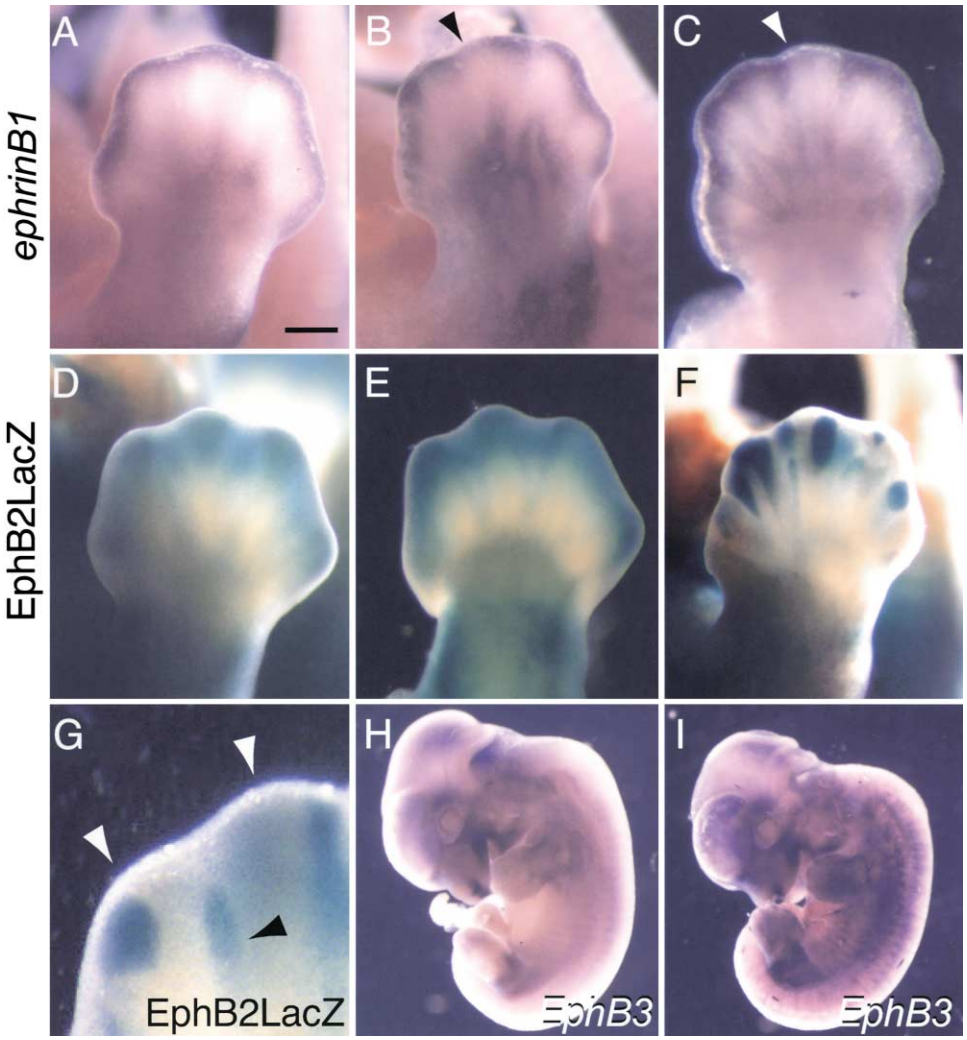

Figure 5. Mosaic Expression of EphrinB1 in Heterozygotes Induces Complementary Eph Receptor Distribution

(A–C) In situ hybridization for *ephrinB1* in Lox (A) and KO/+ (B and C) limbs at E12 (A and B) and E12.5 (C). Note mosaic juxtaposition of *ephrinB1*-deficient (arrowheads) and -positive areas in mutant limbs (B and C).

(D–F) Detection of EphB2 receptor by EphB2LacZ staining in ephrinB1 Lox/+ (D), ephrinB1 KO (E), or ephrinB1 KO/+ (F) animals. The normal spatial distribution of EphB2 expression was maintained in KO embryos, although receptor levels were increased (E), while the pattern was completely altered in KO/+ mutants (F).

(G) In cases of polydactyly (white arrowheads), EphB2-positive domains (black arrowhead) were found centrally between bifurcations.

(H and I) Whole-mount in situ hybridization for *EphB3* on wild-type (H) and KO/+ (I) embryos at E12. *EphB3* transcript distribution was mosaic. Scale bar represents 250 μm in (A)–(F), 100 μm in (G), and 1 mm in (H) and (I). In (A)–(G), anterior corresponds to left and posterior corresponds to right.

as confirmed by studies in zebrafish embryos (Mellitzer et al., 1999; Xu et al., 1999). In mosaic KO/+ limbs, we found evidence for reduced cell mixing between mosaic areas of mesenchyme expressing EphB receptors and ephrinB1, respectively. We hypothesize that EphB-ephrinB1 signaling interfaces provided interacting cells with repulsive cues, which, when properly located, led to diverging cell movements and the splitting of growing digits.

Unusual Phenotypic Inheritance of X-Linked Defects

The ephrinB1 KO/+ phenotype represents a mixed loss-of-function, i.e., the absence of normal receptor-ligand signaling, and gain-of-function scenario, i.e., the formation of ectopic interaction sites, in which the resulting morphogenetic abnormalities surpass the defects seen in full knockouts. Remarkably, similar examples of unusual phenotypic inheritance have been described for certain human X-linked congenital diseases. Julberg-Heilman syndrome is an X-linked dominant disorder that spares male carriers, while females are affected by epilepsy and mental retardation (Ryan et al., 1997). Similarly, in craniofrontonasal syndrome (CNFS), female patients show multiple skeletal malformations, whereas the genetic defect causes no or mild morphological abnormalities in male relatives (OMIM 304110; Feldman et al., 1997). Although some of the abnormalities in

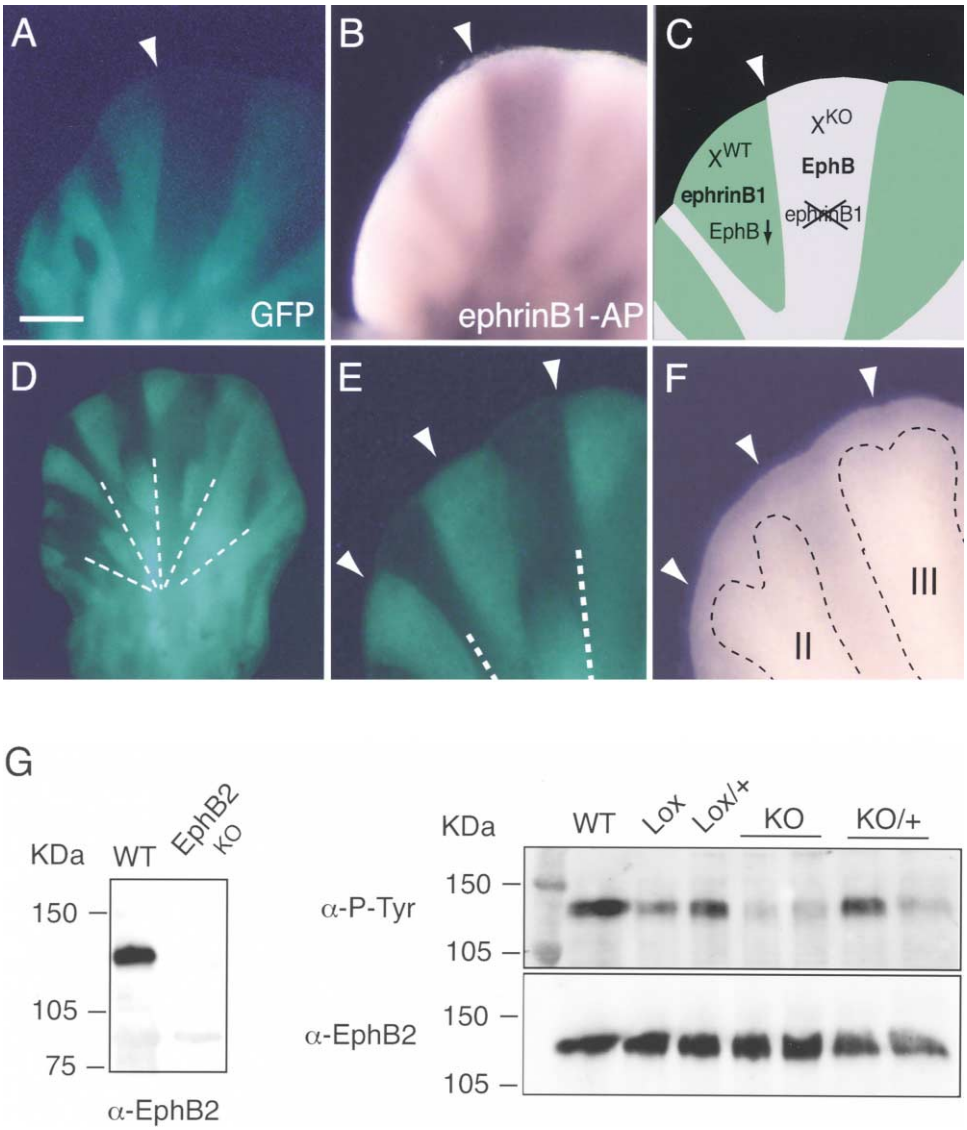

Figure 6. Digit Duplications in KO/+ Mice Correspond to Interfaces between EphrinB1-Expressing and -Deficient Cells

(A and B) Freshly dissected E12 limbs of ephrinB1 KO/+ limbs in which one X chromosome was labeled by GFP (X-GFP). GFP-positive cells used the X chromosome with the wild-type ephrinB1 allele. Conversely, GFP-negative domains in KO/+ limbs lacked ephrinB1 but expressed EphB receptors, as demonstrated by ephrinB1-AP staining (B). The new Eph-ephrin signaling interface was positioned in the middle of a bifurcation forming at digit II (arrowhead).

(C) Schematic representation of the mosaic situation and EphB/ephrinB1 expression in the limb shown in (A) and (B).

(D–F) Freshly dissected E12 limbs of X-GFP/ephrinB1 KO/+ limbs. Dotted lines indicate the position of digital rays in (D) and (E).

(E and F) Higher magnification of distal limbs are shown. Digit bifurcations (indicated by arrowheads and outlined digits) correlated directly with interfaces between ephrinB1-expressing (GFP-positive) and EphB-expressing (GFP-negative) areas.

(G) Analysis of EphB2 activation in ephrinB1 mutant embryos. Left panel, EphB2 was immunoprecipitated from E12.5 embryos and detected by anti-EphB2 antibody (R & D) as an ~120 KDa band. EphB2 KO embryos were used as negative control. Upper right panel; immunoprecipitation of EphB2 receptor from E12 embryos with the indicated genotype, and detection of tyrosine phosphorylation by 4G10 antibody. Lower right panel; EphB2 total protein levels.

Scale bar represents 160 μm in (A) and (B), 250 μm in (D), and 110 μm in (E) and (F). Anterior corresponds to left and posterior corresponds to right.

ephrinB1 KO/+ mice are reminiscent of symptoms seen in CNFS patients, we are not aware of evidence supporting a direct link between the ephrin and the congenital disease. CNFS (Xp22; Feldman et al., 1997) and the *ephrinB1* gene (Xq12) have been mapped to different positions on the human X chromosome. However, the phenotype of ephrinB1 mice provides an example as to how mosaic expression of an X-linked gene can affect its biological function and lead to more severe defects in heterozygous female mutants. Thus, it should be worth investigating whether the unusual severity of heterozygote phenotypes in disorders such as Julberg-Heilman

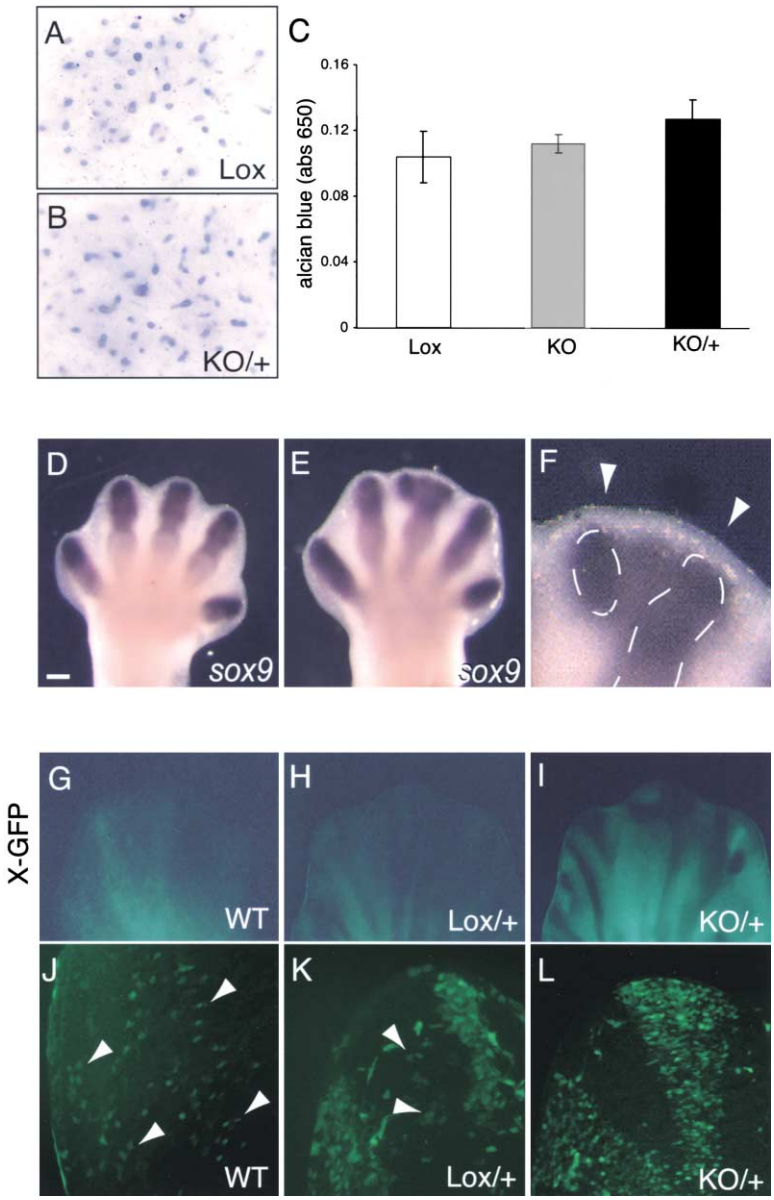

Figure 7. Normal Chondrogenesis, but Reduced Cell Intermingling, in EphrinB1 KO/+ Mesenchyme

(A and B) The four limbs from E12 mutant embryos were pooled for high-density micromass cultures, and chondrogenesis was assessed by alcian blue staining 72 hr after plating. Examples showing comparable numbers of nodules in Lox or KO/+ limbs are shown (A and B).

(C) Quantification of chondrogenesis in Lox (white bar), KO (gray bar), and KO/+ (black bar) limb cultures after 48 hr. The graph shows averages of triplicates and of three independent experiments (5–6 embryos per genotype in total).

(D–F) In situ hybridization for *sox9* on E12.5 wild-type (D) and KO/+ limbs (E and F).

(F) The dotted lines highlight the two areas of higher *sox9* signal corresponding to the two forming digits (arrowheads). Weaker staining was seen in the area enclosed by the bifurcation. Whole-mount fluorescence (G–I) and tangential 7 μm sections (J–L) of wild-type (G and J), Lox/+ (H and K), and KO/+ (I and L) limbs. Note the diffuse GFP signal and the presence of GFP-positive scattered cells in WT embryos and, to a lesser extent, in Lox/+ sections (arrowheads). In contrast, ephrinB1-expressing and -deficient domains were neatly demarcated in KO/+ limbs. Dispersed GFP-positive endothelial cells were visible underneath the AER in both KO/+ and Lox/+ sections.

Scale bar represents 180 μm in (D) and (E), 72 μm in (I), and 120 μm in (J)–(L). Anterior corresponds to left and posterior corresponds to right.

syndrome and CNFS may be attributable to changes in cell adhesion and sorting imposed by the clonal pattern of X inactivation.

Experimental Procedures

Generation of Mutant Mice

LoxP recognition sites for the Cre recombinase from bacteriophage P1 were inserted around the second exon of the murine *ephrinB1* gene. The human *ephrinB1* cDNA was fused in-frame to exon 2 with a conserved ScaI restriction site (amino acid sequence at the fusion site is -YEY|YKL-), and the bovine growth hormone polyadenylation signal sequence was inserted downstream of the cDNA. The targeting construct contained a neomycin resistance cassette surrounded by frt sites to allow Flp recombinase-mediated removal, as well as a 10.5 kb (5′) long arm and a 1.1 kb (3′) short arm for homologous recombination (Figure 1A). After electroporation into E14.1 embryonic stem (ES) cells and selection in G418-containing medium, clones were isolated and characterized by PCR and Southern blot hybridization. A 360 bp probe corresponding to exon 4 was PCR amplified with the primer pair 5′-GGCCATTCTTAGCCCACC TAA-3′ (sense) and 5′-GAAACTCTCTGGGTTCCTGCCT-3′ (antisense) and recognized a 9 kb genomic HindIII fragment in untargeted wild-type ES cells. Two clones were identified in which the size of the ephrinB1 HindIII fragment was increased to 10.5 kb because of homologous recombination (Figure 1B). Several chimeras were obtained after ES cell injection into mouse blastocysts, and lines for both clones were successfully established.

The frt-flanked neomycin (Neo) resistance cassette was subsequently removed by crossbreeding of one conditional ephrinB1 mutant line and transgenic mice expressing Flp recombinase (Dymecki, 1996), but the presence (ephrinB1^{Lox}) or absence (ephrinB1$^{Lox\text{-}Neo}$) of the *Neo* gene did not show any influence on survival or phenotype of the *ephrinB1*-deficient mice described below.

Imunofluorescence on Tissue Sections

Detection of ephrinB1, EphB2, and EphB3 on paraffin sections was performed with goat anti-EphrinB1 (1:200), anti-EphB2 (1:400), and anti-EphB3 (1:100) (all from R & D Systems) antibodies as previously described (Batlle et al., 2002).

Whole-Mount In Situ Hybridization and LacZ Staining

Embryos were collected between E10.5 and E13 in PBS and fixed overnight in 4% paraformaldehyde at 4°C. Whole-mount in situ hybridization was performed as published by Riddle et al. (1993). DIG-RNA probes were hybridized at 70°C overnight and incubated with anti-DIG-AP Fab fragment (Roche). NBT/BCIP substrates (Roche) were used to detect the signal.

For LacZ staining, embryos were fixed in 0.2% glutaraldehyde, 5 mM EGTA, and 2 mM $MgCl_2$ for 10–15 min, washed in 2 mM $MgCl_2$ and 0.02% NP-40, and incubated up to 12 hr at 37°C in staining solution (2.12 mg/ml potassium ferrocyanide and 1.64 mg/ml potassium ferricyanide) containing 1 mg/ml X-gal.

Whole-Mount TUNEL Staining

Limbs were dissected at E12, fixed for 2 hr at 4°C in 4% paraformaldehyde, and washed in PBS/0.1% Tween (PBT). After treatment with 20 μg/ml proteinase K (Sigma) in PBT for 5 min, limbs were fixed with 0.2% glutaraldehyde/4% paraformaldehyde for 20 min, quenched in fresh 0.1% sodium borohydride, and incubated for 1 hr at 37°C with 1× TdT buffer (Roche; 30 mM Tris, 140 mM cacodylate, and 1 mM $CoCl_2$). The buffer was replaced with the reaction mix containing fluorescin-dUTP and terminal deoxynucleotidyl transferase (TdT), according to the manufacturer's instructions (Roche), for 2 hr at 37°C. Samples were extensively washed and photographed under a fluorescent microscope.

Detection of Proliferation by Anti-Phosphohistone H3 Immunofluorescence

Limbs at E12 were dissected, fixed in 4% paraformaldehyde, incubated in sucrose, and embedded in freezing medium (Cryomatrix; Thermo Shandon). Twenty-five micrometer cryosections were washed in PBT, blocked in 5% FCS for 2 hr, and incubated with a polyclonal antibody (1:500; Upstate Biotechnology) detecting phosphorylated serine 10 in histone H3. After washes in PBT, anti-rabbit Alexa 546 (1:800; Molecular Probes) was used as secondary antibody.

Skeletal Preparations

For staining of cartilage and bone, E18.5 embryos were skinned, eviscerated, and fixed in 100% ethanol for 4 days. Samples were incubated in acetone and stained for 10 days in a solution containing 0.3% alcian blue 8GX (Sigma), 0.1% alizarin red S (Sigma), acetic acid, and ethanol in a ratio of 1:1:1:17. Specimens were kept in 20% glycerol/1% potassium hydroxide until tissue had completely cleared.

Cartilage at E13 was detected by overnight incubation of freshly dissected limbs in 0.1% alcian blue 8GX/0.1N HCl and then clearing in 20% glycerol/1% potassium hydroxide.

Western Blot Analysis and Immunoprecipitation

E12.5 embryos were lysed in 10 mM Tris, 150 mM NaCl, and 1%Triton X-100. One milligram of total protein lysate was incubated with wheat germ lectin-Sepharose beads 6MB (Sigma) for several hours in rotation at 4°C. Beads were washed repeatedly and loaded on an SDS acrylamide gel, and ephrinB1 protein was detected by a rabbit polyclonal antiserum (Bruckner et al., 1997). Signal was developed with ECL detection reagents (Amersham).

For immunoprecipitation, E12.5 embryos were lysed in 1 ml PLC buffer (50 mM HEPES [pH 7.5], 150 mM NaCl, 10% glycerol, 1.5 mM $MgCl_2$, 1 mM EGTA, 0.1% Triton X-100, and 1% NP-40) containing 1 mM sodium orthovanadate. Two milligrams of lysate were immunoprecipitated with 1 μg of goat anti-EphB2 antibody (R & D Systems). Samples were repeatedly washed with PLC buffer and loaded on an SDS acrylamide gel. Phosphotyrosine levels were assessed by staining with 4G10 antibody (Upstate; 1:1000). Blots were stripped and reprobed with anti-EphB2 antibody (1 μg/ml).

High-Density Limb Cultures and Alcian Blue Staining of Chondrogenic Nodules

E12 limbs were dissected, pooled, and disaggregated at 37°C in 0.1% collagenase (Sigma) and 0.1% trypsin (Invitrogen). Disaggregation was stopped by addition of 15% FCS DMEM medium, and the suspension was washed twice in fresh medium. Finally, cells were resuspended in a suitable volume and diluted to 2.5×10^5 cells/10 μl. A 10 μl cell drop was positioned in the center of each well in a 24-well dish, allowed to attach for 2 hr, and then floated with 15% FCS DMEM medium. Culture medium was exchanged daily, and differentiation was evaluated after 48–72 hr by fixing for 10 min in 4% formaldehyde and then by overnight staining in 0.1% alcian blue 8GX/ 0.1N HCl. Cultures were rinsed in water and photographed, and the dye was extracted in 200 μl of 6 M guanidine hydrochloride (Sigma) for quantification (absorbance at 650 nm). Samples were plated in triplicates.

Whole-Mount Detection of Eph Receptors by AP Fusion Proteins

EphrinB1-AP secreted protein was produced by transient transfection of 293 cells and collection of conditioned medium over three days. Embryos were incubated with ephrinB1-AP overnight, washed extensively, and fixed for 10 min with 60% acetone, 3.7% formaldehyde, and 20 mM HEPES. Endogenous alkaline phosphatase was inactivated for 2 hr at 65°C. The presence of surface-bound AP fusion proteins was detected by NBT/BCIP substrates.

Acknowledgments

The authors thank D. Duboule, C. Dickson, N. Brockdorff, and A. Nagy for reagents and transgenic mice, K. Vintersten and F. Diella for technical support, and J. Lewis and N. Vargesson for reading the manuscript. This work was funded by Cancer Research UK, an EMBO long-term fellowship to A.C., the EMBO Young Investigator Programme (R.H.A.), and the Deutsche Forschungsgemeinschaft (R.K.).

Received: May 5, 2003
Revised: May 29, 2003
Accepted: June 5, 2003
Published: August 11, 2003

References

Avner, P., and Heard, E. (2001). X-chromosome inactivation: counting, choice and initiation. Nat. Rev. Genet. *2*, 59–67.

Batlle, E., Henderson, J.T., Beghtel, H., van den Born, M.M.W., Sancho, E., Huls, G., Meeldijk, J., Robertson, J., van de Wetering, M., Pawson, T., and Clevers, H. (2002). β-Catenin and TCF mediate cell positioning in the intestinal epithelium by controlling the expression of EphB/ephrinB. Cell *111*, 251–263.

Bouillet, P., Oulad-Abdelghani, M., Vicaire, S., Garnier, J.M., Schuhbaur, B., Dolle, P., and Chambon, P. (1995). Efficient cloning of cDNAs of retinoic acid-responsive genes in P19 embryonal carcinoma cells and characterization of a novel mouse gene, Stra1 (mouse LERK-2/Eplg2). Dev. Biol. *170*, 420–433.

Bruckner, K., Pasquale, E.B., and Klein, R. (1997). Tyrosine phosphorylation of transmembrane ligands for Eph receptors. Science *275*, 1640–1643.

Capdevila, J., and Izpisua Belmonte, J.C. (2001). Patterning mechanisms controlling vertebrate limb development. Annu. Rev. Cell Dev. Biol. *17*, 87–132.

Chen, J.M. (1952). Studies on the morphogenesis of the mouse sternum. I. Normal embryonic development. J. Anat. *86*, 373–386.

Dymecki, S.M. (1996). Flp recombinase promotes site-specific DNA recombination in embryonic stem cells and transgenic mice. Proc. Natl. Acad. Sci. USA *93*, 6191–6196.

Feldman, G.J., Ward, D.E., Lajeunie-Renier, E., Saavedra, D., Robin, N.H., Proud, V., Robb, L.J., Der Kaloustian, V., Carey, J.C., Cohen, M.M., Jr., et al. (1997). A novel phenotypic pattern in X-linked inheritance: craniofrontonasal syndrome maps to Xp22. Hum. Mol. Genet. *6*, 1937–1941.

Flenniken, A.M., Gale, N.W., Yancopoulos, G.D., and Wilkinson, D.G. (1996). Distinct and overlapping expression patterns of ligands for

Eph-related receptor tyrosine kinases during mouse embryogenesis. Dev. Biol. *179*, 382–401.

Hadjantonakis, A.K., Cox, L.L., Tam, P.P., and Nagy, A. (2001). An X-linked GFP transgene reveals unexpected paternal X-chromosome activity in trophoblastic giant cells of the mouse placenta. Genesis *29*, 133–140.

Hall, B.K., and Miyake, T. (2000). All for one and one for all: condensations and the initiation of skeletal development. Bioessays *22*, 138–147.

Henkemeyer, M., Orioli, D., Henderson, J.T., Saxton, T.M., Roder, J., Pawson, T., and Klein, R. (1996). Nuk controls pathfinding of commissural axons in the mammalian central nervous system. Cell *86*, 35–46.

Kullander, K., and Klein, R. (2002). Mechanisms and functions of Eph and ephrin signalling. Nat. Rev. Mol. Cell Biol. *3*, 475–486.

Lallemand, Y., Luria, V., Haffner-Krausz, R., and Lonai, P. (1998). Maternally expressed PGK-Cre transgene as a tool for early and uniform activation of the Cre site-specific recombinase. Transgenic Res. *7*, 105–112.

Logan, M., Martin, J.F., Nagy, A., Lobe, C., Olson, E.N., and Tabin, C.J. (2002). Expression of Cre recombinase in the developing mouse limb bud driven by a Prxl enhancer. Genesis *33*, 77–80.

Martin, J.F., and Olson, E.N. (2000). Identification of a prx1 limb enhancer. Genesis *26*, 225–229.

Mellitzer, G., Xu, Q., and Wilkinson, D.G. (1999). Eph receptors and ephrins restrict cell intermingling and communication. Nature *400*, 77–81.

Orioli, D., Henkemeyer, M., Lemke, G., Klein, R., and Pawson, T. (1996). Sek4 and Nuk receptors cooperate in guidance of commissural axons and in palate formation. EMBO J. *15*, 6035–6049.

Riddle, R.D., Johnson, R.L., Laufer, E., and Tabin, C. (1993). Sonic hedgehog mediates the polarizing activity of the ZPA. Cell *75*, 1401–1416.

Ryan, S.G., Chance, P.F., Zou, C.H., Spinner, N.B., Golden, J.A., and Smietana, S. (1997). Epilepsy and mental retardation limited to females: an X-linked dominant disorder with male sparing. Nat. Genet. *17*, 92–95.

Shubin, N.H., and Alberch, P. (1986). A morphogenic approach to the origin and basic organization of the tetrapod limb. Evol. Biol. *20*, 319–387.

Stadler, H.S., Higgins, K.M., and Capecchi, M.R. (2001). Loss of Eph-receptor expression correlates with loss of cell adhesion and chondrogenic capacity in Hoxa13 mutant limbs. Development *128*, 4177–4188.

Storm, E.E., and Kingsley, D.M. (1996). Joint patterning defects caused by single and double mutations in members of the bone morphogenetic protein (BMP) family. Development *122*, 3969–3979.

Vargesson, N., Clarke, J.D., Vincent, K., Coles, C., Wolpert, L., and Tickle, C. (1997). Cell fate in the chick limb bud and relationship to gene expression. Development *124*, 1909–1918.

Wilkinson, D.G. (2001). Multiple roles of EPH receptors and ephrins in neural development. Nat. Rev. Neurosci. *2*, 155–164.

Xu, Q., Mellitzer, G., Robinson, V., and Wilkinson, D.G. (1999). In vivo cell sorting in complementary segmental domains mediated by Eph receptors and ephrins. Nature *399*, 267–271.